ORIGINAL ARTICLE

Detection of pancreatic islet allograft impairment in advance of functional failure using magnetic resonance imaging

J. Kriz,[1] D. Jirak,[2] Z. Berkova,[1] V. Herynek,[2] A. Lodererova,[3] P. Girman,[1] D. Habart,[1] M. Hajek[2] and F. Saudek[1]

1 Diabetes Center, Institute for Clinical and Experimental Medicine, Prague, Videnska, Czech Republic
2 Department of Diagnostic and Interventional Radiology, Institute for Clinical and Experimental Medicine, Prague, Videnska, Czech Republic
3 Department of Pathology, Institute for Clinical and Experimental Medicine, Prague, Videnska, Czech Republic

Summary

This study evaluated the ability of magnetic resonance imaging (MRI) to predict failure of pancreatic islets (PI) transplanted into the hepatic portal vein. Brown-Norway ($n = 18$) and Lewis ($n = 6$) rats received islets isolated from Lewis donors. The rejection process in Brown-Norway recipients was mitigated by two different immunosuppressive regimens [tacrolimus + hydrocortisone for 3 months ($n = 6$) or tacrolimus for 12 days ($n = 12$)]. Longitudinal MRI monitoring of recipients at post-transplantation weeks 1, 2, 3, 4, 6, 8, 10, and 12 confirmed the ability to detect SPIO labeled PI after transplantation into the liver. The relative number of MRI signals related to PI isografts remained stable up to study completion. Recipients of PI allografts were normoglycemic until the end of study; signals declined gradually to $44 \pm 17\%$ in these animals. In animals with islets failure during post-transplant week 12, the number of signals decreased to $25 \pm 10\%$ of initial values. The difference between groups (islet function/failed) became significant post-transplant week 3. Our data demonstrate that the MRI changes attributable to rejection become apparent within 3 weeks after transplantation, i.e. at least 8 weeks before functional allograft failure.

Introduction

Transplantation of allogeneic pancreatic islets (PI) represents a promising treatment for patients with type-1 diabetes mellitus [1]. Its application is limited by several factors, including immediate coagulative damage and delayed rejection of allogeneic tissue [2–5]. Worldwide, transplant researchers continue to investigate possible improvements in techniques of islets isolation, preservation, transplantation, and long-term recipient care. Fundamental for the evaluation of such improvements is a method for *in vivo* visualization of islet distribution and viability. Considerable attention has been paid to the adaptation of current imaging techniques, such as magnetic resonance imaging (MRI), positron emission tomography (PET), and bioluminescence [6–9]. Until recently, optimal imaging methods of islets transplanted into the portal vasculature have been lacking. PET in combination with computed tomography (CT) made it possible to study short-term islet survival and distribution in the liver [8,10]. However, only MRI has enabled the detection of transplanted islets during the months following transplantation with sufficient sensitivity and spatial resolution [11–14].

We [13], and others [12,14] demonstrated the possibility of islet labeling with superparamagnetic iron oxide (SPIO)-based contrast agents without any obvious detrimental effect on beta-cell function, and the subsequent

detection of islets transplanted into the liver or beneath the kidney capsule using MRI [11,12,14–17]. The SPIO-labeled intra-hepatically transplanted islet isografts remain visible on MRI scans as distinct hypointense areas for at least 24 weeks [13]. Rapid failure of the allogeneic islets because of rejection is followed by a gradual disappearance of the signal on MRI scans [18]. However, it still remains unclear whether longitudinal MRI monitoring can be used to detect islet rejection even before functional islet failure is manifested by hyperglycemia. This early detection is a prerequisite for a clinically meaningful graft salvage intervention.

In a fully allogeneic model without immunosuppression, islet failure proceeds rapidly, and MRI does not detect islet injury early enough to allow for graft-saving intervention [16]. In the present study, we mitigated rejection after allogeneic islet transplantation into streptozotocin-induced diabetic rats by two different immunosuppressive protocols. Transplanted and control animals were monitored using MRI over a period of 12 weeks to evaluate the early phase of transplanted islet rejection. Our data demonstrate that the MRI changes attributable to rejection become apparent within 2–3 weeks after transplantation, when the graft is still able to maintain normal glucose tolerance in the diabetic animals.

Methods

Study design

The control Group-A ($n = 6$) was transplanted with syngeneic islets and did not receive any immunosuppression. Two groups of diabetic recipients of allogeneic PI (Group-B, $n = 6$; Group-C, $n = 12$) were treated with two different immunosuppressive regimens. At the end of study, the animals in Group-C were divided into two subgroups (C1, $n = 6$; C2, $n = 6$) according to allograft function. In all three groups, marginal islet number [19,20] was transplanted to shorten the silent period of rejection before the onset of hyperglycemia. In all animals, sequential MRI was performed weekly during the first month and biweekly over the next 2 months (Fig. 1a). Chemical diabetes was induced in all recipients by intravenous injection of streptozotocin (50 mg/kg; Sigma-Aldrich, St. Louis, MO, USA) and confirmed by hyperglycemia over 18 mmol/l on three consecutive measurements. Nonfasting glycemia was monitored every other day for 2 weeks after transplantation and subsequently twice a week until study completion. At the twelfth week, an intravenous glucose tolerance test was performed, all animals were killed, and liver samples for histology were excised. Destruction of the majority of islet B cells was verified after termination of the experiment by measuring total insulin content in transplant recipient
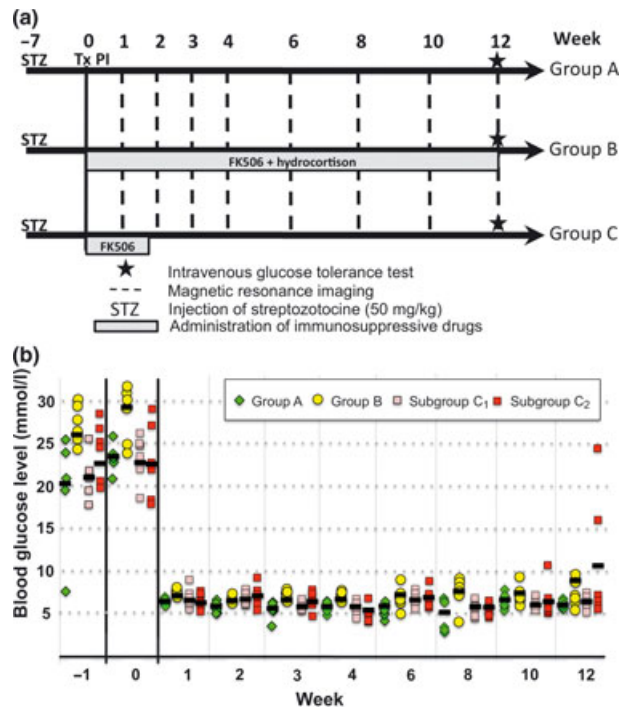
Figure 1 (a) Study design – Lewis and Brown-Norway rats were treated with intravenously injected streptozotocin (50 mg/kg) 7 days prior to islet transplantation. Recipients with confirmed diabetes were divided into three groups. Group-A included recipients (Lewis rats) of islet isografts without any concomitant medication. Animals in Groups-B and -C (Brown-Norway rats) were treated with transplantation of allogeneic pancreatic islets followed by transient (Group-C) or indefinite (Group-B) immunosuppression. All animals were examined using MRI scanner 1, 2, 3, 4, 6, 8, 10, and 12 weeks after transplantation. Graft function was tested by IVGTT performed on week 12. (b) Blood glucose levels – Blood glucose was measured in all animals throughout the study. Individual glycemias measured on days of MRI scanning are shown. All recipients of Groups -A, -B, and -C1 remain normoglycemic until study completion. Two animals of Subgroup-C2 became hyperglycemic during week 12.

pancreases. Explanted organs were frozen in liquid nitrogen and mechanically pulverized. Processed tissue was then exposed to glacial acetic acid overnight and spun at 68 000 *g*. Total content of insulin in the supernatant was measured using radioimmunoassay (^{125}I RIA Kit; ICN Pharmaceuticals, Costa Mesa, CA, USA).

Animals

The donors of PI were adult male Lewis rats (weight 250–280 g). The recipients in Groups-B and -C were the Brown-Norway rats (weight 200–240 g) and recipients in Group-A were Lewis rats (weight 220–250 g). All animals were kept according to the European Convention on Animal Care with free access to food pellets and water. The

Animal Care Committee of the Institute for Clinical and Experimental Medicine and Ministry of Health of Czech Republic approved all protocols related to this study.

Rat PI isolation and labeling

Pancreatic islets were isolated as previously described [21]. Briefly, after intraductal collagenase injection (1 mg/ml; Sevapharma, Prague, Czech Republic), the distended pancreas was excised and gently shaken at 37 °C for 20 min. Islets were separated from exocrine tissue using centrifugation in discontinuous Ficoll® gradient (Sigma, St. Louis, MO, USA). The isolated islets were then cultured for 48 h in CMRL-1066 medium (PANBiotech GmbH, Aidenbach, Bavaria, Germany) supplemented with 10% fetal calf serum, 1% penicillin/streptomycin/L-glutamine, 1% HEPES (all from Sigma-Aldrich), and MRI contrast agent ferucarbotran (5 μl/ml, Resovist®; Schering AG, Berlin, Germany) in an incubator at 37 °C and 5% CO_2 atmosphere. The labeling efficiency was confirmed using MRI of gelatin phantoms ($n = 4$). Thirty labeled islets were individually laid out on the 4% gelatin bottom layer and subsequently covered by 3% gelatin upper layer. The number of islets was compared with number of detected hypointense regions.

Functional testing of islets before transplantation

A representative sample of each set of the transplanted islets was tested for glucose-stimulated insulin production. Samples of 50 islets in doublets were incubated in Kreb's solution with consecutive glucose levels of 3.3 and 22.0 mmol/l. Insulin concentration in the medium was measured after a 60 min incubation at each glucose concentration, using a specific RIA kit (ImmuChem Coated Tube Insulin ^{125}I RIA Kit; MP Biomedicals, Solon, OH, USA) in duplicates. Stimulation indexes were calculated as the ratio of stimulated and basal concentrations and compared with unlabeled islet controls obtained from the same preparation.

Isolated islet transplantation

Just before transplantation, the islets were removed from the labeling culture, carefully washed from the free contrast agent (HBSS + 1% fetal calf serum), handpicked and collected into 1 ml syringes. Using a 24G catheter inserted into the portal vein all islets were injected into the liver of totally anesthetized recipients (flunitrazepam 0.1 mg/kg i.v. + ketamine 10 mg/kg i.m.). Lewis rats were injected with 2000 islets (minimal number of islets necessary for normalization of blood glucose levels). Brown-Norway rats, which are considerably more sensitive to insulin, received 1000 islets.

Immunosuppressive regimens

In Group-B, a combination of tacrolimus (0.5 mg/kg/day i.m.) and hydrocortisone (2 mg/kg/day i.m.) was initiated at day 1 after transplantation and continued 5 days a week for a total of 12 weeks. In Group-C, tacrolimus alone (0.5 mg/kg/day; i.m.) was injected daily to rats and stopped at day 12 following transplantation. Trough levels of tacrolimus in whole blood were tested 24 h after previous dose application in each group at day 10 after the transplantation using IMx Tacrolimus Assay (Abbott, Abbott Park, IL, USA). Based on our previous experience the dose was targeted to trough blood levels of 5–15 ng/ml.

In vivo MRI

In all recipients, sequential MRI was performed at 1, 2, 3, 4, 6, 8, 10, and 12 weeks following transplantation, using an experimental 4.7 Tesla spectrometer BioSpec equipped with a resonator coil (Bruker, Rheinstetten, Germany). During the scanning procedure, animals were restrained by general gas anesthesia (Isoflurane®; Torrex Pharma, Wien, Austria). A standard T2*-weighted gradient echo sequences were applied with repetition time 80 ms, echo time 3.4 ms, slice thickness 1 mm, number of slices 20, number of acquisitions 4, field of view 6 cm and matrix 256×256 pixels. Total amount of hypointense regions related to transplanted islets was manually calculated in all sections covering the liver area of each recipient. The number determined by the first examination 1 week after transplantation was considered as 100%. Results of subsequent scans were expressed as a percentage of this initial quantity.

Intravenous glucose tolerance test (IVGTT)

Intravenous glucose tolerance test was performed at week 12 in all animals. After study completion, transplant recipients in Group-C were divided according to their IVGTT outcomes into Subgroup-C1 ($n = 6$) with $K_G \geq 1.20$%/min and Subgroup-C2 ($n = 6$) with $K_G < 1.19$%/min.

Histology and immunohistochemistry

Animals were terminated after the last MRI. Livers were excised and fixed for histological grading of rejection. Tissue fixed in 10% buffered formalin for 24 h was divided into 10 parts and embedded in paraffin for histology and combined iron and insulin detection. Ten 4 μm thick sections prepared from each liver were de-paraffinized in xylene and rehydrated in graded ethanol.

Routine hematoxylin-eosin staining was performed on all samples followed by detection and basic assessment of islets rejection. Slices for detection of insulin positive cells were prepared from liver samples with the confirmed presence of transplanted islets. An artificially high background signal was prevented by endogenous peroxidase and biotin neutralization by 0.3% H_2O_2 in 70% ethanol and with a biotin blocking system (Dako-Cytomation, Glostrup, Denmark). These tissue samples were incubated with primary anti-insulin antibody (Sigma-Aldrich), which was detected using Histofine Simple Stain Rat MAX PO (NICHIREI, Tokyo, Japan). After incubation with Dako liquid DAB + substrate-chromogen system, the specimens were submerged in a freshly prepared Pearl's Prussian blue solution (2% hydrochloric acid mixed with 2% potassium ferrocyanide). After washing out, these sections were counterstained with nuclear fast red.

Statistical analysis

Statistical analysis was performed using GraphPad Prism version 3.00 (GraphPad Software, La Jolla, CA, USA). Total quantity of hypointense regions was assessed in all 20 MRI slices covering the entire liver volume. The decrease in the number of the islet spots was calculated for each animal separately relative to its individual starting value obtained at the first week after transplantation. Islet signal counts on the subsequent scans were expressed as a percent of this initial count in each rat. The trends of relative numbers of the islet spots were compared among all groups using ANOVA with repeated measurements and grouping factor followed by the Neuman–Kuels multiple comparison test. Relative decrease of signals related to the transplanted tissue within groups was assessed by the paired Wilcoxon test. Absolute numbers of spots between groups were compared using the Mann–Whitney test. Spearman correlation was used to assess the relation between the coefficients of glucose assimilation and the absolute numbers of detected islet MRI signals. Total amounts of insulin detected within pancreases of recipients were compared by one-way ANOVA. A *P*-value <0.05 was considered significant.

Results

In vitro verification of the function of labeled islets

The mean stimulation indexes obtained from the ferucarbotran-labeled and nonlabeled islets were 7.33 ± 3.94 and 8.16 ± 6.70, respectively. This difference was not significant (*P* = 0.33; Wilcoxon test), indicating that islet labeling by ferucarbotran did not impair *in vitro* insulin secretion.

Islet function in the mitigated rejection model

In all streptozotocin-induced diabetic rats (Groups-A, -B and -C), nonfasting blood glucose levels were normalized (<9 mmol/l) within 3 days after islet transplantation. Normal nonfasting blood glucose level was maintained until study completion in all animals of the control syngeneic Group-A and in the allogeneic Group-B. IVGTT, a more sensitive functional indicator, showed full islet function in all animals of Groups-A and -B ($K_G \geq 1.2\%$/min), indicating the effectiveness of the intensive immunosuppressive regimen. In contrast, two recipient rats from the allogeneic Group-C, which received a less intensive immunosuppressive regimen, became hyperglycemic by week 12, indicating graft failure (Fig. 1b). Impaired islet function was detected by IVGTT in four additional animals in this group. The average insulin content in pancreases measured in all islet recipients at the end of the study was 70.3 ± 36.9 mIU. This corresponds to less than 10% of the amount found in 11 healthy control BN rats (1156 ± 350 mIU).
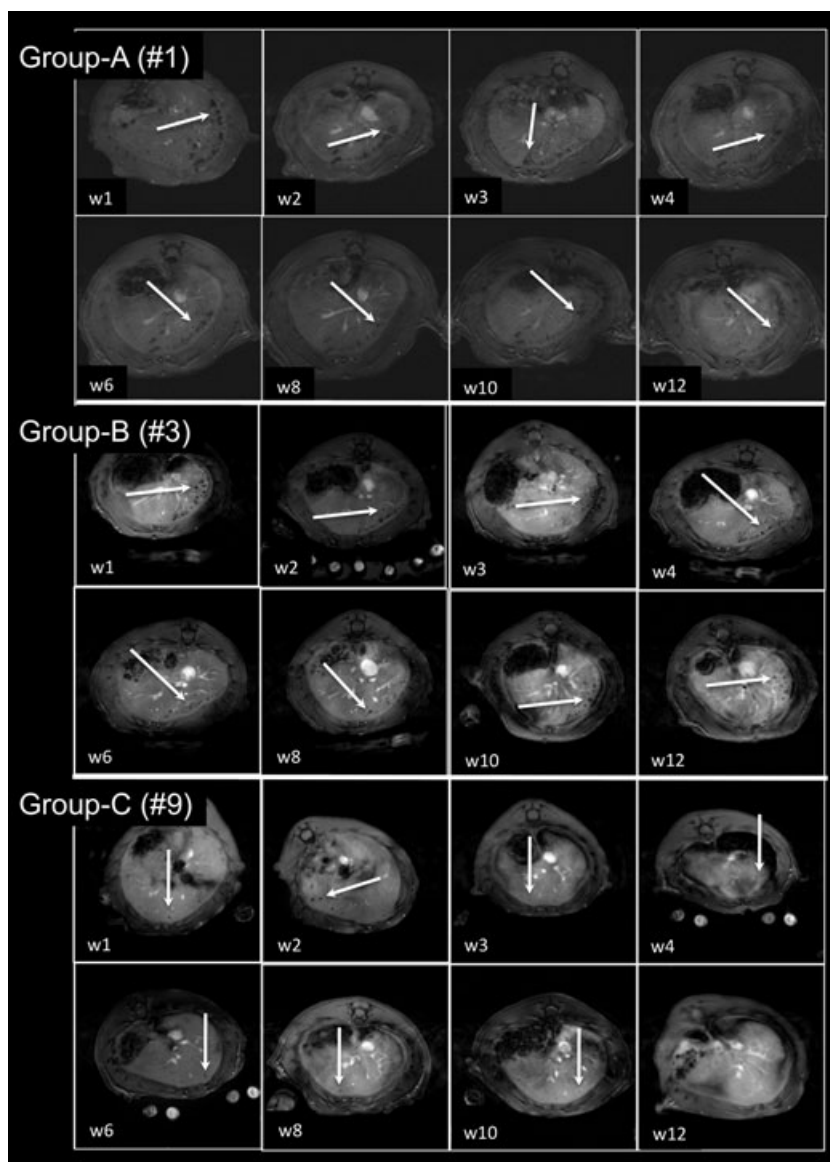
MRI of SPIO labeled islets

A total of 119 hypointense spots were detected in gelatin phantoms, which contained 120 PI labeled by Resovist® for 48 h.

The first examination of animals was performed at week 1 after complete recovery from the surgical procedure and establishment of normoglycemia. The 20 MRI slices covered the target region of recipient body during every examination. In 12 of 20 MRI slices the liver tissue was detected, as seen in Fig. 2. An additional eight slices showed the abdominal cavity just adjacent to the liver. In allogeneic animals treated with 1000 labeled islets (Groups-B and -C), we detected an average of 264 ± 88.9 (range, 106–378) hypointense regions. This number did not differ significantly from that of the syngeneic Lewis group (A), which received 2000 syngeneic islets (264 ± 67.4; range, 130–396).

Twelve weeks after transplantation, the mean total number of islet-related signals in Group-A was 242 (SD ± 72.8). In Groups-B and -C, the mean numbers of the islet-related spots were 101 (SD ± 26) and 103 (SD ± 49), respectively. The differences between recipients of syngeneic and allogeneic islets were statistically significant (A vs. B and A vs. C both *P* < 0.01).

Trends of islet spot disappearance among groups

The mean values of the relative spot number for groups at each time point were calculated. From these values the trends over the time period of 12 weeks were determined.

Figure 2 Representative T2* weighted MRI of recipient livers. Typical images of animals treated with labeled islet allografts and isografts were chosen. The hypointense regions related to transplanted islets are visible as dark, rounded spots within the liver tissue (white arrows). Panels a–c show corresponding layers of animal #1 of Group-C, animal #3 of Group-B, and animal #9 of Subgroup C2 (graft failed at week 12). MRI was performed at weeks 1, 2, 3, 4, 6, 8, 10, and 12 after transplantation of islets into the portal vein. The number of hypointense spots representing islet isografts was stable, as can be seen in animal #1 of Group-A. Hypointense regions related to islet allografts gradually disappeared until the study completion (animal #3 of Group-B, and animal #9 of Subgroup C2).

Figure 3 depicts this statistical analysis and shows that trends between groups varied significantly (ANOVA with repeated measurements, A vs. B: $P < 0.01$, A vs. C, $P < 0.001$; B vs. C, $P < 0.05$). In the syngeneic control Group-A, the mean number of islet signals decreased insignificantly to $91 \pm 2.67\%$ of the initial value during the 12 week follow-up period. In fact, this decrease occurred only between the first and the second week after transplantation (Fig. 3). In the allogeneic Groups-B and -C, the number of islet signals gradually dropped to $50 \pm 14\%$ and $34 \pm 17\%$ of the original value, respectively. The loss of islet-related hypointense spots was detected in all animals in Groups-B and -C, and the loss occurred progressively up to study completion.

Early identification of islet rejection by MRI

Group-C was divided according to the K_G values at the end of the study into Subgroup-C1 ($n = 6$) and Subgroup-C2 ($n = 6$). The final mean number of islet spots was $44 \pm 17\%$ in Subgroup-C1 and $25 \pm 11\%$ in Subgroup-C2 ($P < 0.05$, Mann–Whitney test). In animals treated by allogeneic transplantation, an obvious drop in islet spot count was observed early after transplantation. In animals that finally achieved the preset normal K_G value ($\geq 1.2\%$/min) this drop was not significant until week 3 ($P < 0.05$); in animals with impaired islet function ($K_G < 1.2\%$/min) the drop was already significant at week 2 ($P < 0.001$; Wilcoxon paired test).
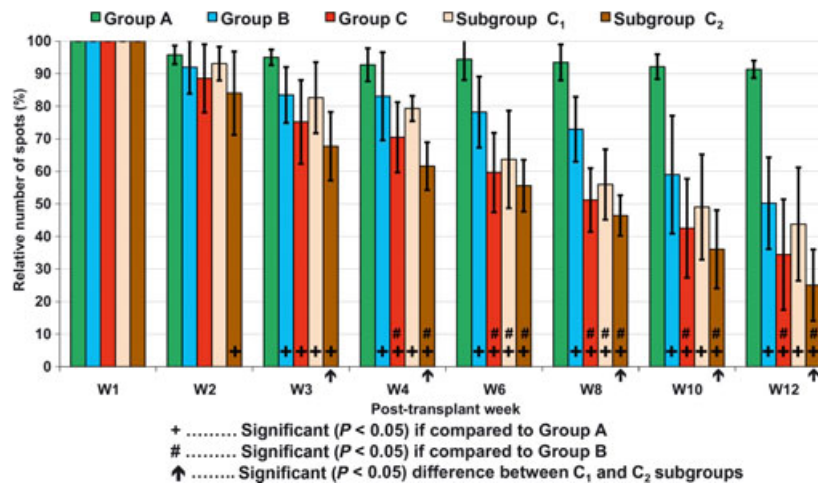
Figure 3 Relative numbers of hypointense spots representing transplanted islets. Relative numbers of hypointense spots detected in Groups-A, -B, and C during 12 post-transplant weeks are shown. Nonspecific processes caused a slight decline in detected spots to $91 \pm 2.67\%$ in animals of Group-A during weeks 1 and 2 after transplantation. Without the influence of acute rejection, the signals related to islet isografts remained stable until study completion. As a result of the combined effects of moderated rejection and nonspecific processes, the mean number of spots in Groups-B and -C gradually dropped to $50 \pm 14.07\%$ and $34 \pm 16.97\%$, respectively, at week 12. If compared with animals of Group-A, the decline was significantly faster in Group-B ($P < 0.01$). The fastest disappearance of hypointense spots was detected in Group-C (A vs. C, $P < 0.001$; B vs. C, $P < 0.05$). Animals of Group-C were divided into two subgroups according to K_G calculated from IVGTT performed at week 12. The number of hypointense spots decreased significantly faster ($P < 0.05$) in animals with impaired or failed allografts (Subgroup C2; $n = 6$). The significant decreases (irrespective of reason) within groups with failed and functional grafts were detected in the second and the third weeks, respectively. The influence of acute rejection characterized by a difference of detected spots among groups of animals treated by isografts and functional or failed allografts became significant ($P < 0.05$) at weeks 4 or 3, respectively. Thus, the significant decline of spots on MRI was detected at least 8 weeks before allograft functional failure (C2; $n = 6$).

The changes in MRI were particularly apparent from weeks 1–3. Figure 4a shows the course of weekly changes in relative numbers of islet signals in the individual groups. There were no significant differences in the syngeneic group compared with initial state. Decline of signal from allogeneic islets happen mainly during the first 3 weeks and then continued at a slower rate. The relative signal loss (compared with week 1) detected in islet allograft recipients at week 3 correlates with the IVGTT-K_G values measured at the end of study [Fig. 4b; negative linear correlation coefficient of -0.51 ($P = 0.003$)].

Histological verification of the rejection process

Transplanted islets in the liver samples were distributed either individually (Fig. 5a, b, c, d, and f) or grouped in clusters (Fig. 5e), which were presumably detected by MRI as a single dark region. Prussian blue staining of liver sections taken at week 12 from all recipients confirmed the presence of the iron particles within islets. Liver samples taken from Group-A revealed well-preserved structure of the islet isografts. No lymphocytic infiltration was detectable in the total of 20 islets from six animals (Fig. 5a), and each showed apparent abundant

insulin production (Fig. 5d). In contrast, islet allografts of Groups-B and -C demonstrated clear signs of acute rejection. The islets detected in the liver samples taken from six animals of Group-B and six animals of Subgroup-C1 revealed partially preserved morphology of islet allografts (Fig. 5b, black arrow) with some insulin positive cells and lymphoid infiltration (Fig. 5b dotted arrow, E). All 35 tested islets in the liver samples taken from six recipients of Subgroup-C2 showed severe impairment of islet structure and massive lymphoid infiltration (Fig. 5c,f) related to acute rejection.

Discussion

Currently, high resolution MRI is the only noninvasive method capable of detecting transplanted PI in the liver over a prolonged period of time [22,23]. To discriminate islets from surrounding tissue, they must be *in vitro* labeled either with positive or negative contrast agents, which are incorporated into the islet cells during *in vitro* culture. Thus, far only superparamagnetic iron oxide nanoparticles have been used in clinical trials [24,25]. Iron oxide crystals present in the islet cells cause local signal loss on T2* weighted MRI, which can be seen as a
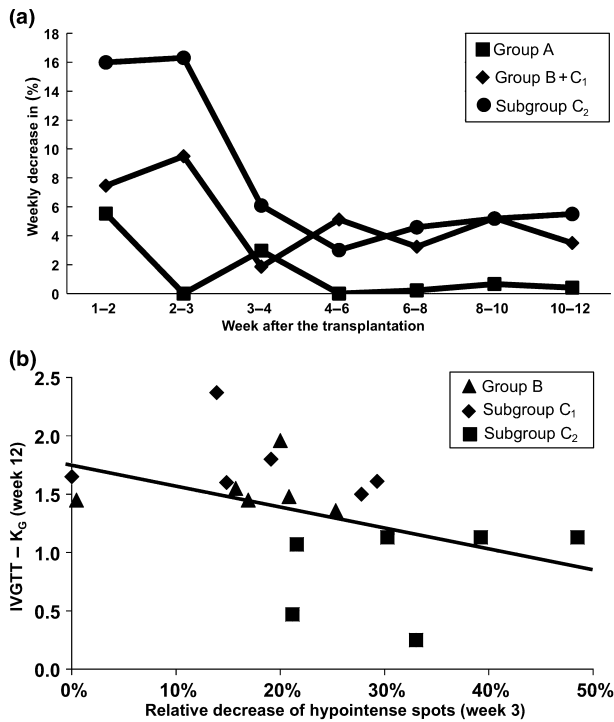
Figure 4 Decline of islet-related spots and graft function. (a) A weekly decreases of hypointense spots detected in animals of Group-A and animals with functional (Group-B + Subgroup-C1) and failed (Subgroup-C2) allografts are shown. The declines of signals detected in Subgroup-C2 happen mainly during the first 3 weeks and then continued at a low rate. (b) There is a negative linear correlation (Spearman correlation test; $P = 0.003$, $r = -0.51$) between early (3 weeks after transplantation) relative decline of hypointense spots representing transplanted islet allografts and late (at study completion) function of allografts.

distinct rounded dark spots corresponding to individual or grouped islets [16]. The safety of β-cell labeling in terms of *in vitro* as well as *in vivo* vitality and the ability to release insulin has been documented for two clinically approved iron-based MRI contrast agents: ferucarbotran (Resovist®, Schering AG) [11,26] and ferumoxide (Endorem®, Guerbet S.A., Villepinte, France; Feridex®, AMAG Pharmaceuticals, Inc., Lexington, MA, USA) [27]. Serial MRI might thus be used for longitudinal monitoring of the islet graft especially with regard to early diagnosis of rejection.

According to previously published studies [11,13,14,16,26] and in the present investigation of labeled phantoms, practically all types of islet cells incubated for 48 h with ferucarbotran had cytoplasmic endosomes containing iron nanoparticles. *In vitro* MRI of islet phantoms were proven to detect islets with 100% sensitivity. Commonly, it is important to take into account presumed variable efficiency of cells in incorporating the

contrast agent and resultant inconsistent total quantity of iron accumulated within individual islets. More iron uptake produces larger and more intensive signal loss (darker color) in MRI, but in the current study only the number of hypointense spots, irrespective of area or color intensity, was calculated. The highly sensitive molecular MRI combined with superparamagnetic iron oxide nanoparticles allows visualization to the level of individual cells [28,29]. Therefore, sensitivity limits of MRI are not an issue in quantitation of detected islets. When used for *in vivo* visualization, MRI detects much fewer signals related to prelabeled islets. Despite the fact that cells of all 2000 islets contain SPIO nanoparticles, the total number of hypointense spots corresponded to approximately 250 per animal 1 week after transplantation. It is supposed that some of islets were destroyed immediately following transplantation and their SPIO nanoparticles were metabolized and thus inactivated as a contrast agent. Further decline in the number of visible signals is caused by extremely strong susceptibility of the superparamagnetic iron nanoparticles, which leads to overlapping of spots, particularly if the islets are grouped in clusters (Fig. 5e). This so-called "blooming artifact" is logically more frequent when more islets are transplanted into the same volume.

The direct connection between rapid disappearance of signals detected by MRI and immune destruction of islet allografts or xenografts has been demonstrated by several research groups including ours [12,14,16,18]. In the present study, we first showed that serial MRI monitoring of recipients can detect the rejection-induced decline in spots related to islets far in advance of their functional failure. In the syngeneic islet transplant group, the total number of islet spots decreased on average by 10% between the first and second post-transplant weeks, but then remained stable (as well as glucose control) over a 3-month period. In an allogeneic model with either sustained or only temporary immunosuppression, MRI detected gradual signal loss, which showed significant inverse correlation with IVGTT results. The number of islet signals was considerably lower in Subgroup-C2 whose islet graft finally failed or showed an impaired glucose tolerance test. The intensity of rejection predicted by MRI examination was confirmed by histology at study completion.

Nevertheless, the incomplete elimination of SPIO particles in spite of a total rejection of islet cells is reported by several authors [15,16,30]. In accordance with this, our preliminary immunohistochemical data show that ferucarbotran nanoparticles need not stay in the endocrine cells permanently following transplantation. They can persist in resting macrophages and other cells of the host origin and can give a false hypointense MRI signal [30].
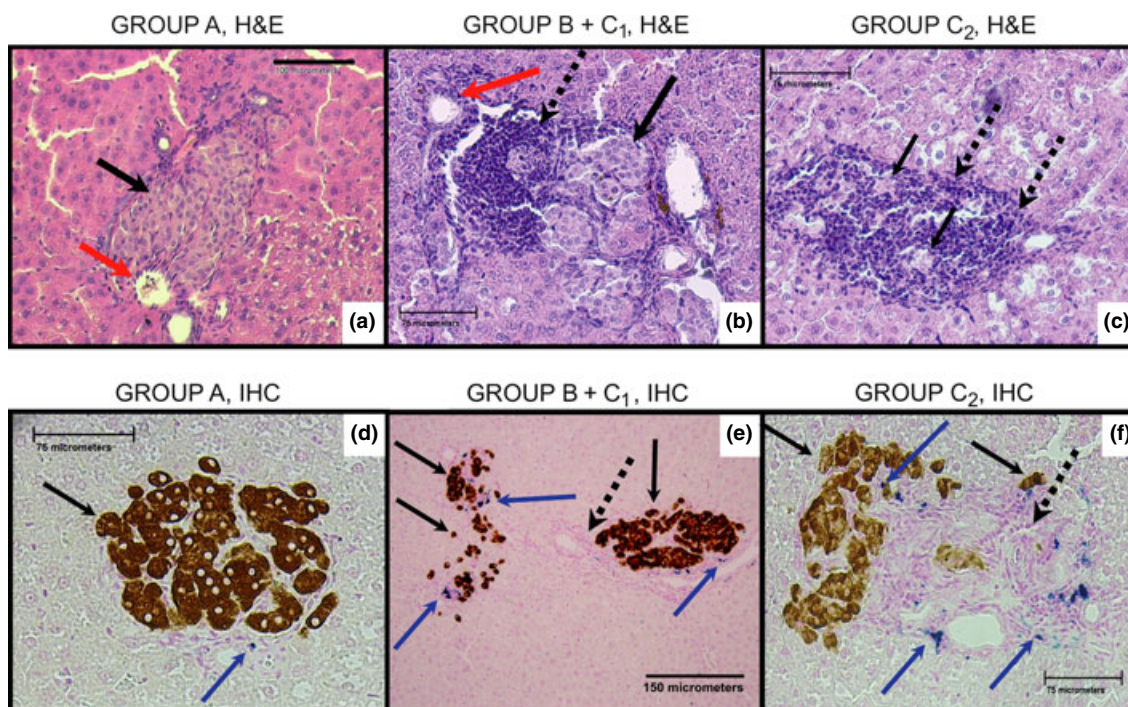
Figure 5 Microscopic examination of recipient livers. Microscopically examined samples of recipient livers confirmed the presence of transplanted islets distributed individually (a, b, c, d, f) or grouped in clusters (e). Hematoxylin-eosin (HE; a, b, c) and immunohistochemistry (IHC; d, e, f) staining revealed well-preserved structure of islet isografts (a, black arrow) located close to small vessels (red arrow). Within islet region are numerous insulin positive cells (d, black arrow) and iron positive particles (d, blue arrow). In case of isografts there is not any lymphoid infiltration. Partially preserved islets (b, black arrow) with some insulin positive cells (e, black arrow) and some lymphoid cells (b, e dotted arrow) were detected in recipients of Group-B and Subgroup C1. Several iron positive particles were detected close to insulin positive cells (e, blue arrows). Severe impairment of structure and massive lymphoid infiltration (c, f dotted arrow) related to acute rejection were typical for liver samples taken from recipients of Subgroup-C2. Prussian blue staining confirmed the presence of iron particles within islets. Only a few insulin positive cells were detected.

Intravenously injected ferucarbotran (in a clinical approved dosing) rapidly accumulates within resident liver macrophages (Kupffer cells), which efficiently eliminate it during over several days [13]. Jirak *et al.* demonstrated in a murine model that SPIO overdosing (two times the correct dose) leads to oversaturation and consequent inability of Kupffer cells to decompose SPIO nanoparticles over the course of more than 4 weeks [31]. In currently reported and in previously published experiments the iron (SPIO) concentration in islet cells [1 µl of tissue = 1.5–20.7 µg Fe; (12,13)] substantially exceeds the iron concentration within liver tissue during clinical examination [1 µl of tissue = 20 ng Fe (32,33)]. Thus, there is a risk oversaturation of surrounding macrophages by rapidly released SPIO. Despite this, the hypointense signal related to the SPIO labeled islets dramatically decreased during the first two post-transplant weeks. Evgenov *et al.* reported a 45% decline in the number of hypointense spots [15] and Jirak *et al.* reported a 50% decrease in the hypointense signal [18] during the first week after transplantation of SPIO labeled islets in mice. If we take into account well known data concerning the

massive destruction of islet cells immediately after infusion into the portal vein [8], we can suppose that the ischemic necrosis of islets and surrounding liver tissue stimulates Kupffer cells. These strongly stimulated macrophages presumably can decompose SPIO nanoparticles even if they are released excessively from destroyed islets. On the other hand, a longitudinal MRI monitoring of SPIO labeled islet isografts showed that there is also an initial dramatic decrease of signal followed by a period when the absolute number of hypointense spots remained stable over the course of several months. Nevertheless, its area and color intensity gradually decreased over time [16,18]. This confirms that SPIO particles slowly leaking from islet cells can be metabolized similarly to SPIO particles used in clinical practice. Kupffer cells, even without any special stimulation, can inactivate them. Rapid release of SPIO combined with high activation of Kupffer cells or slow release of SPIO combined with nonactivated of Kupffer cells results in effective decomposition of SPIO nanoparticles. We can deduce that there is a delicate balance between the intensity of release of SPIO particles from islet cells and the level of Kupffer cell activation.

Several authors reported less than 50% engrafted tissue after the first post-transplant week [8,15,18]. In the current experiments, acute cellular rejection was moderated with a potent immunosuppressive therapy. Therefore, in recipients of Group-C with failed grafts, the weekly decline of islets number (i.e. released SPIO nanoparticles) could be up to 5%. Surrounding Kupffer cells most likely can effectively process this amount of SPIO nanoparticles. Therefore, false positive signals in MRI are not expected.

Without supportive immunosuppressive therapy, the rat islet allografts typically maintain normal blood glucose levels for only 10–14 days after transplantation [16]. Most islets that survive the first post-transplant week are rapidly destroyed during the second week and consequently a considerable amount of SPIO nanoparticles is released. We can hypothesize that the stimulation of macrophages by simple cellular rejection is not strong enough for efficient decomposition of suddenly released SPIO nanoparticles. These can presumably persist insitu and provide false hypointense signal. Our data together with this hypothesis convince us that our monitoring is efficient over a period of three post-transplant months, when the risk of islet rejection is high.

The initial numbers of detected hypointense spots were comparable both in animals transplanted with 1000 allografts and those receiving 2000 isografts. Although this disproportion might have been ascribed to the nonspecific anti-inflammatory effects of the immunosuppressive drugs, we think this more likely caused by the above-mentioned "blooming artifact". This is also why, for the long-term study, the relative and not absolute numbers of islet signals were compared. Our data suggest that in a model of moderated islet rejection the MRI changes attributable to rejection become apparent already at 2–3 weeks after transplantation, still within the period when the islet graft is able to maintain normal glucose tolerance in diabetic recipients. For prediction of the fate of the islet graft, it is important to perform MRI assessment within 3–4 weeks post-transplant, when a decrease of the relative number of islet spots correlates fairly well with islet survival over the next several months. Although in our study the number of observations was limited, we assume that at least for our model a 30% decrease from the initial value represents an important finding. To consider these data absolutely robust, it should be compared with islets quantitation by a generally accepted morphological method that could be used as a reference value. Microscopic morphometry is extremely time consuming if performed using whole liver samples or should be considered an approximation only. Therefore, results obtained by MRI can be correlated only indirectly to functional parameters or to limited histological data.

A disadvantage of this form of follow-up is that the data provides only a relative numbers of islet spots, although this drawback could possibly be improved by better standardization of the labeling process [27]. In addition, the current method of evaluation is rather laborious, particularly if we aim to identify every labeled islet or islet cluster. Although this is still possible in small rodents, it would be impossible in humans and a sophisticated automated methods to define the liver area and summarize the total quantity of the islet spots will be needed [17,18]. It might be more applicable with complex methods using a double contrast to define the liver volume (e.g. by i.v. gadolinium administration [34]) or by visualization of SPIO-labeled PI as a positive contrast using the echo-dephased steady-state free precession technique [35,36]. To what extent this technique might be useful for the diagnosis of rejection using MRI of the SPIO-labeled islets in human patients remains to be established in ongoing clinical studies [24].

For *in vivo* visualization of transplanted islets in humans, PET in combination with CT has been introduced [10,37]. This technique is promising in the evaluation of islets several hours after implantation, but will not be useful for long-term monitoring with regard to the rather low elimination half time of the β-radiation of tracers. For diagnosis of rejection, bioluminescence has been successfully used, but this method would not be applicable for humans [38].

The lack of noninvasive techniques allowing for early diagnosis of rejection and well-timed initiation of anti-rejection therapy represents a major drawback of current islet transplant protocols. As pilot clinical studies focused on noninvasive imaging of iron-labeled PI using MRI are already underway, our experimental findings may help to interpret the results and to design future research in this area.

Authorship

JK: designed and performed surgical part of the research, analyzed data, wrote the article. DJ: performed most of the MRI monitoring, analyzed data, edited the manuscript. ZB: performed some of the surgical interventions, collected data. VH: performed some of the MRI monitoring. AL: optimized and performed microscopic examinations. PG: performed some of the surgical interventions, collected data. DH: edited the manuscript. MH: supervised the imaging portion of the study, analyzed data. FS: general supervision, study design, manuscript editing.

Funding

References

1. Shapiro AM, Lakey JR, Ryan EA, *et al.* Islet transplantation in seven patients with type 1 diabetes mellitus using a glucocorticoid-free immunosuppressive regimen. *N Eng J Med* 2000; **343**: 230.

2. Davalli AM, Scaglia L, Zangen DH, Hollister J, Bonner-Weir S, Weir G. Vulnerability of islets in the immediate posttransplantation period dynamic changes in structure and function. *Diabetes* 1996; **45**: 1161.

3. Merani S, Shapiro AM. Current status of pancreatic islet transplantation. *Clin Sci (Lond).* 2006; **110**: 611.

4. Ryan EA, Paty BW, Senior PA, *et al.* Five-year follow-up after clinical islet transplantation. *Diabetes* 2005; **54**: 2060.

5. Shapiro AM, Hao EG, Lakey JR, *et al.* Novel approaches toward early diagnosis of islet allograft rejection. *Transplantation* 2001; **71**: 1709.

6. Biancone L, Crich SG, Cantaluppi V, *et al.* Magnetic resonance imaging of gadolinium-labeled pancreatic islets for experimental transplantation. *NMR Biomed* 2007; **20**: 40.

7. Chen X, Zhang X, Larson CS, Baker MS, Kaufman DB. *In vivo* bioluminescence imaging of transplanted islets and early detection of graft rejection. *Transplantation* 2006; **81**: 1421.

8. Eich T, Eriksson O, Sundin A, *et al.* Positron emission tomography: a real-time tool to quantify early islet engraftment in a preclinical large animal model. *Transplantation* 2007; **84**: 893.

9. Fowler M, Virostko J, Chen Z, *et al.* Assessment of pancreatic islet mass after islet transplantation using *in vivo* bioluminescence imaging. *Transplantation* 2005; **79**: 768.

10. Eich T, Eriksson O, Lundgren T. Visualization of early engraftment in clinical islet transplantation by positron-emission tomography. *N Eng J Med* 2007; **356**: 2754.

11. Berkova Z, Jirak D, Zacharovova K, *et al.* Labeling of pancreatic islets with iron oxide nanoparticles for *in vivo* detection with magnetic resonance. *Transplantation* 2008; **85**: 155.

12. Evgenov NV, Medarova Z, Dai G, Bonner-Weir S, Moore A. *In vivo* imaging of islet transplantation. *Nat Med* 2006; **12**: 144.

13. Jirak D, Kriz J, Herynek V, *et al.* MRI of transplanted pancreatic islets. *Magn Reson Med* 2004; **52**: 1228.

14. Tai JH, Foster P, Rosales A, *et al.* Imaging islets labeled with magnetic nanoparticles at 1.5 Tesla. *Diabetes* 2006; **55**: 2931.

15. Evgenov NV, Medarova Z, Pratt J, *et al. In vivo* imaging of immune rejection in transplanted pancreatic islets. *Diabetes* 2006; **55**: 2419.

16. Kriz J, Jirak D, Girman P, *et al.* Magnetic resonance imaging of pancreatic islets in tolerance and rejection. *Transplantation* 2005; **80**: 1596.

17. Kriz J, Jirak D, White DJ, Foster P. Magnetic resonance imaging of pancreatic islets transplanted into the right liver lobes of diabetic mice. *Transpl Proc* 2008; **40**: 5.

18. Jirak D, Kriz J, Strzelecki M, *et al.* Monitoring the survival of islet transplants by MRI using a novel technique for their automated detection and quantification. *MAGMA* 2009; **22**: 9.

19. Girman P, Kriz J, Dovolilova E, Cihalova E, Saudek F. The effect of bone marrow transplantation on survival of allogeneic pancreatic islets with short-term tacrolimus conditioning in rats. *Ann Transplant* 2001; **6**: 43.

20. Kriz J, Saudek F, Girman P, Novota P. Enhancement of rat islet tolerance with bone marrow transplantation using a non-myeloablative procedure II: failure despite the presence of lymphocyte microchimerism in the fully allogeneic Lewis/Brown-Norway model. *Int J Tissue React* 2004; **26**: 75.

21. Gotoh M, Maki T, Kiyoizumi T, Satomi S, Monaco AP. An improved method for isolation of mouse pancreatic islets. *Transplantation* 1985; **40**: 437.

22. Medarova Z, Moore A. MRI as a tool to monitor islet transplantation. *Nat Rev Endocrinol* 2009; **5**: 444.

23. Saudek F, Brogren CH, Manohar S. Imaging the Beta-cell mass: why and how. *Rev Diabet Stud* 2008; **5**: 6.

24. Toso C, Vallee JP, Morel P, *et al.* Clinical magnetic resonance imaging of pancreatic islet grafts after iron nanoparticle labeling. *Am J Transplant* 2008; **8**: 701.

25. Saudek F, Jirak D, Girman P, *et al.* Magnetic resonance imaging of pancreatic islets transplanted into the liver in humans. *Transplantation* 2010; **90**: 1602.

26. Berkova Z, Kriz J, Girman P, *et al.* Vitality of pancreatic islets labeled for magnetic resonance imaging with iron particles. *Transpl Proc* 2005; **37**: 3496.

27. Malosio ML, Esposito A, Poletti A, *et al.* Improving the procedure for detection of intrahepatic transplanted islets by magnetic resonance imaging. *Am J Transplant* 2009; **9**: 2372.

28. Heyn C, Bowen CV, Rutt BK, Foster PJ. Detection threshold of single SPIO-labeled cells with FIESTA. *Magn Reson Med* 2005; **53**: 312.

29. Heyn C, Ronald JA, Ramadan SS, *et al. In vivo* MRI of cancer cell fate at the single-cell level in a mouse model of breast cancer metastasis to the brain. *Magn Reson Med* 2006; **56**: 1001.

30. Zacharovova K, Berkova Z, Herynek V, *et al. Post-transplantation Processing of Magnetic Iron Nanoparticles in Rat Pancreatic Islets.* 28th Workshop of the AIDPIT Study Group of EASD, abstract no. IE17, p 41. Austria: Igls, 2009.

31. Jirak D. *Free SPIO Injected into the Kidney and Liver*. Toronto: ISMRM, 2008.

32. Zhu JY, Leng XS, Dong N, Qi GY, Du RY. Measurement of liver volume and its clinical significance in cirrhotic portal hypertensive patients. *World J Gastroenterol* 1999; **5**: 525.

33. Heilmaier C, Lutz AM, Bolog N, Weishaupt D, Seifert B, Willmann JK. Focal liver lesions: detection and characterization at double-contrast liver MR imaging with ferucarbotran and gadobutrol versus single-contrast liver MR imaging. *Radiology* 2009; **253**: 724.

34. Herynek V, Berkova Z, Dovolilova E, *et al.* Improved detection of pancreatic islets *in vivo* using double contrast. *Contrast Media Mol Imaging* 2011; **6**: 308.

35. Patil S, Bieri O, Scheffler K. Echo-dephased steady state free precession. *MAGMA* 2009; **22**: 277.

36. Patil S, Jirák D, Saudek F, Hájek M, Scheffler K. Positive contrast visualization of SPIO-labeled pancreatic islets using echo-dephased steady-state free precession. *Eur Radiol* 2011; **21**: 214.

37. Toso C, Zaidi H, Morel P, *et al.* Positron-emission tomography imaging of early events after transplantation of islets of Langerhans. *Transplantation* 2005; **79**: 353.

38. Chen X, Zhang X, Larson C, Xia G, Kaufman DB. Prolonging islet allograft survival using *in vivo* bioluminescence imaging to guide timing of antilymphocyte serum treatment of rejection. *Transplantation* 2008; **85**: 1246.